



An Assessment of the Use of Mesoporous Silica Materials to Improve Pulsed Dipolar Spectroscopy

Yei-Chen Lai¹ · Albert Chang¹ · Chia-Min Yang¹ · Yun-Wei Chiang¹ 

Received: 26 April 2018 / Revised: 5 July 2018 / Published online: 13 July 2018
© Springer-Verlag GmbH Austria, part of Springer Nature 2018

Abstract

Protein immobilization in mesoporous silica nanoparticles has attracted much attention due to its wide range of applications. However, it remains largely unexplored how the use of mesopores can alter the spatial distribution of encapsulated biomolecules so as to improve pulsed dipolar spectroscopy sensitivity. Here, we performed electron spin resonance measurements for three different spin-labeled biomolecules (including two different peptides and a protein) encapsulated in various types of mesoporous materials differing in textural properties such as nanochannel length (e.g., 0.2–4 μm) and average pore diameter (e.g., 6–11 nm, approximately). Our results show that biomolecules are clustered somewhat upon the encapsulation into mesopores, and that due to the clustering, instantaneous diffusion plays an important role in the spin relaxation in nanochannels. The extent of molecular clustering exhibits a clear positive correlation with the length of nanochannels, whereas it shows little correlation with pore diameters. Among the materials studied, mesoporous materials with the shortest length of nanochannels are most effective to reduce spin clustering, thus suppressing the unwanted instantaneous diffusion and enhancing spin–spin relaxation time. This study has opened a possibility of improving the quality of pulsed dipolar spectroscopy with mesoporous silica nanoparticles.

1 Introduction

Mesoporous silica materials with high specific surface area and well-ordered pore structures are of interest for a wide range of applications. The immobilization and encapsulation of proteins in mesoporous materials has been extensively investigated due to great potential applications, such as improving immobilized

Electronic supplementary material The online version of this article (<https://doi.org/10.1007/s00723-018-1040-z>) contains supplementary material, which is available to authorized users.

✉ Yun-Wei Chiang
ywchiang@gapp.nthu.edu.tw

¹ Department of Chemistry, National Tsing Hua University, Hsinchu 30013, Taiwan

enzyme activity/selectivity and serving as a carrier of protein drugs [1–3]. The porous structure provides a protective environment for proteins such that protein stability against denaturing effects can, in some cases, be enhanced [4–7]. However, it remains largely unexplored as to how the spatial distribution and arrangement of the guest biomolecules are affected by the textural properties of host mesoporous materials. The development of methods capable of counting molecules and characterizing the spatial distribution of guest molecules in mesoporous materials has been long desired [8].

Site-directed spin-labeling (SDSL) electron spin resonance (ESR) techniques have been established as a powerful tool for determining structure and topology of protein and protein complex [9–11]. In SDSL-ESR spectroscopy, the introduction of a paramagnetic nitroxide side chain is accomplished through cysteine-substitution mutagenesis. The nitroxide molecule serves as a probe of local environment, hence providing site-specific information about local dynamics and ordering in protein. SDSL-ESR has also been proven useful in studying interfacial hydration and backbone dynamics along a polypeptide (or even a protein) confined in mesoporous materials [12–14]. The local environment in nanochannels has been studied by pulsed ESR techniques and found that the nanoconfined environment can maintain solvent in an amorphous state suitable for studying protein structure and dynamics at low temperatures [15]. However, a systematic study of how the immobilized proteins are redistributed in nanochannels according to the differences in textural property of materials has yet to be reported.

The present study, therefore, aims to assess the use of mesoporous materials to improve the measurement of pulsed dipolar spectroscopy in the aspects of optimizing phase memory spin–spin relaxation time of spin-labeled biomolecules by modulating the textural properties of mesoporous materials. We report an investigation of how the textural properties of mesoporous materials affect the spatial distribution of spin-labeled biomolecules using pulsed ESR techniques. Various mesoporous materials with differences in hexagonal platelet morphologies, average pore diameters, and nanochannel length are prepared to host spin-labeled biomolecules, including two different types of polypeptides and one protein. The local concentration of the encapsulated biomolecules is determined from the measurements by double electron–electron resonance (DEER) technique and then compared with the result of bulk solvent. As a result, we provide a quantitative description of how the spatial distribution of the guest biomolecules is affected by the textural properties of the mesoporous materials. The information is potentially valuable to the use of mesoporous materials for maximizing pulsed dipolar spectroscopy sensitivity. Besides, we measure the spin-echo relaxation time (T_m) of the samples in various mesoporous materials using electron spin-echo (ESE) technique. Taken together the DEER and ESE measurements, a linear relation is revealed from the plot of $1/T_m$ versus the measured local spin concentration. The linear relation provides important evidence to support the role of instantaneous diffusion in the spin-labeled biomolecules encapsulated in mesoporous materials.

2 Materials and Methods

2.1 Biomolecule Sample Preparations and Encapsulation

All peptides of this study were custom-synthesized by Kelowna International Scientific Inc. (New Taipei, Taiwan) with purity greater than 95%. n3 peptide is a linear 26-mer polypeptide with a sequence of GNDYEDRYYRENMYRYPN-QVYYRPVA, where the first 25 residues correspond to the domain 142–166 of the human prion protein and the underlined letters represent the segments that correspond to helix H1 and β -strand S2, respectively, in the normal prion structure [16]. It is highly soluble and exhibits an intrinsic propensity to a β -hairpin conformation at neutral pH in the PB buffer (10 mM sodium phosphate, pH 6.5) and in pure water [17]. In this study, the third and ninth sites of n3 peptide were substituted with cysteine and the resulting spin-labeled mutant was denoted as n3-d. PP-s is a 14-mer-long polyproline model peptide, with the seventh residue substituted with cysteine. Each peptide had an acetylated N terminus and an amidated C terminus.

To prepare the recombinant Bid proteins, the full-length mouse Bid was cloned into *NdeI/XhoI* site of pET28a vector (New England Biolabs, Inc.) and then transformed into the *E. coli* BL21(DE3) expression strain (Novagen). The recombinant proteins fused with six-histidine residues at the N terminus were expressed and purified by an affinity Ni column, as previously described [18]. Briefly, bacterial culture was grown at 37 °C in Luria–Bertani medium containing kanamycin (30 $\mu\text{g}/\text{mL}$) until OD600 reached 0.6–0.8. Protein expression was induced by addition of 1 mM of IPTG (isopropyl 1-thio- β -D-galactopyranoside) at 30 °C for 4–6 h. The cell pellet was collected by centrifugation and resuspended in ice-cold lysis buffer (20 mM Tris, 100 mM NaCl, 20 mM imidazole, pH 7.4 and cOmplete Protease Inhibitor Tablets). The resuspended pellet was sonicated on ice for 5 min, followed by centrifugation at 13,000g for 40 min. The supernatant was filtrated through a 0.22 μm filter and then loaded onto an affinity Ni column using HisTrap HP (GE Healthcare) at a flow rate about 1 mL/min. The column was washed with 10 column volumes of wash buffer (50 mM Tris, 500 mM NaCl, and 40 mM imidazole, pH 7.4). Bid fractions were eluted with ten column volumes of elution buffer-1 (20 mM Tris, 100 mM NaCl, and 100 mM imidazole, pH 7.4) and elution buffer-2 (20 mM Tris, 100 mM NaCl and 500 mM imidazole, pH 7.4). Purified protein was confirmed by sodium dodecyl sulfate–polyacrylamide gel electrophoresis with coomassie blue staining. Imidazole was removed using a PD-10 desalting column (GE Healthcare) equilibrated with storage buffer (20 mM Tris and 100 mM NaCl, pH 7.4), and protein concentration was estimated via absorption spectroscopy at 280 nm.

In the spin-labeling experiments, peptides/proteins were labeled with a tenfold excess of (1-oxy-2,2,5,5-tetramethyl-3-pyrroline-3-methyl) methanethiosulfonate spin label (MTSL) (Alexis biochemicals, San Diego, CA, USA) per cysteine residue for overnight in the dark at 4 °C. They were further purified by reverse phase HPLC as previously described [17]. MALDI-TOF experiments were conducted

to confirm the identity of the peptides. The solution volume used in the bulk solvent study was 40 μL [ca. 0.5 mM in a mixture of 30% glycerol (cryoprotectant) and PB buffer]. The encapsulation of spin-labeled biomolecules into nanochannels was prepared as previously described [13, 15, 19]. Briefly, 20 μL of biomolecule solution was mixed with 12 mg of mesoporous materials, then the sample was directly loaded into a quartz tube (3 mm o.d.) sealed with Parafilm and then sent for ESR measurements. We performed the following experiments to verify that the spin-labeled peptides/proteins were not adsorbed/left on the outer surface of the materials and that the molecules were trapped adequately well within the nanochannels. An excess buffer was added into the ESR tube containing the mesoporous materials. The tube was sent for ESR measurements at room temperature. The collected spectra were found to remain identical to the spectra collected before the addition of the excess buffer; that is, the spectra show typical slow-motional line shapes, indicating the presence of the nanoconfinement effect. This study also confirmed that no ESR signal was obtained for the supernatant liquid after centrifugation. ESR signals were not detected in the supernatant liquid until the materials were incubated in excess buffer for longer than 2 weeks.

2.2 Mesoporous Materials

MSU-H mesoporous silica (abbreviated as MSU) material was purchased from Aldrich. Two different SBA-15 mesoporous silicates were prepared. One is the conventional fiber-like SBA-15 (denoted as SBA-15) purchased from ACS (Advance Chemicals Supplier, USA) and the other is the plate-like SBA-15 (referred to as SBA-15-p) synthesized as previously described [20, 21]. Briefly, tetraethoxysilane (TEOS) was added to a hydrochloric acid (HCl) solution of a triblock copolymer (Pluronic P123, $\text{EO}_{20}\text{PO}_{70}\text{EO}_{20}$) and zirconium oxychloride octahydrate ($\text{ZrOCl}_2 \cdot 8\text{H}_2\text{O}$). The mixture was stirred at 35 $^\circ\text{C}$ for 24 h, further added with sulfuric acid (H_2SO_4), and then aged at 90 $^\circ\text{C}$ for 24 h and then filtered and dried. The molar composition of the final mixture was 1 TEOS:0.017 P123:5.9 HCl:193 H_2O :2.9 H_2SO_4 :0.05 ZrOCl_2 . The final product was further heated to 350 $^\circ\text{C}$ to obtain the calcined sample (denoted as SBA-15-p1). A series of plate-like SBA-15-p-type materials with identical unit cell size, but different pore diameters (i.e.,

Table 1 Textural properties of mesoporous materials

Mesoporous material	Pore diameter (nm)	Unit cell size (nm)	Channel length (μm)
MSU	7.1	11.6	0.5–1
SBA-15	8–10	N.A.	1–4
SBA-15-p1	7.6	11.6	0.2
SBA-15-p2	6.5	13.4	0.2
SBA-15-p3	8.1	13.4	0.2
SBA-15-p4	9.1	13.4	0.2
SBA-15-p5	10.4	13.4	0.2

SBA-15-p2~p5) were prepared following the reported procedures [21]. The textural properties of the mesoporous materials are listed in Table 1.

2.3 Pulsed ESR Measurements

All of the ESR measurements were performed at X-band frequency (9.4 GHz). DEER experiments were carried out using the typical four-pulse constant-time DEER sequence as previously described [13, 22]. The detection pulses were set to 32 and 16 ns for π and $\pi/2$ pulses, respectively, and pump frequency was set to approximately 70 MHz higher than the detection pulse frequency. The pulse amplitudes were chosen to optimize the refocused echo. The $\pi/2$ pulse was employed with $+x/-x$ phase cycle to eliminate receiver offsets. The duration of pumping pulse was about 32 ns, and its frequency was coupled into the microwave bridge by a commercially available setup (E580-400U) from Bruker. All pulses were amplified via a pulsed traveling wave tube amplifier (E580-1030). The field was adjusted, such that the pump pulse is applied to the maximum of the nitroxide spectrum, where it selects the central $m_I=0$ transition of A_{zz} together with the $m_I=0, \pm 1$ transitions. The sample tube was plunge-cooled in liquid nitrogen and then transferred into the ESR probehead (ER4118X-MS3), which was pre-cooled to a desired temperature (50–80 K) using the helium flow system. Accumulation time was 6–10 h at temperature 50–70 K for peptide samples, and 6–9 h at 80 K for protein samples. The ESE experiments were carried out using the Hahn echo sequence [23]. The field was adjusted to optimize the spin echo, and the duration time of $\pi/2$ and π pulses was set to 16 and 32 ns.

2.4 Data Analysis and Theoretical Background

ESE decay signals were fitted to a stretched exponential function in Eq. (1) to extract T_m value from the ESE data [15, 23]:

$$V(2\tau) = V(0) \exp \left[- \left(\frac{2\tau}{T_m} \right)^x \right], \quad (1)$$

where $V(2\tau)$ and $V(0)$ are the echo intensity at time 2τ , twice the time between the two pulses, and echo intensity extrapolated to time zero, respectively. Some examples exhibiting the measurements and analyses are shown in the Online Resource (Figure S1). The parameters x and T_m describe the shape of the echo decay and x depends upon the mechanism of echo dephasing. In many cases, the observed signal decays can be fitted with a simple exponential decay (i.e., $x=1$) [23, 24]. The obtained relaxation rate (i.e., $1/T_m$) can be approximately considered, as a sum of all relaxation mechanisms contributes to the spin-echo dephasing.

The contribution from the molecular motion of spin label itself inducing relaxation is usually minor to the overall spin dephasing at cryogenic temperatures [23]. For nitroxide radicals in the biological system, the following relaxation mechanisms

can possibly be dominant: (1) spin diffusion (contributed from the nearby nuclear spins flip-flop, usually from protons); (2) methyl protons rotation in the environment (especially in the protein buried site); and (3) instantaneous diffusion (controlled inversion of electron spins by a microwave pulse). The contribution of instantaneous diffusion to the spin-echo relaxation is given by

$$\frac{1}{T_{\text{ID}}} = \frac{\pi\mu_0 g_A g_B \mu_B^2}{9\sqrt{3}\hbar} C\lambda, \quad (2)$$

where T_{ID} is the echo dephasing time associated with instantaneous diffusion, μ_0 is the vacuum permeability, $g_{A,B}$ are the effective values of the g -tensors of the spins, μ_B is the Bohr magneton, \hbar is the Planck constant divided by 2π , C is the concentration, and λ is the fraction of excited spins. Accordingly, in the case of high local spin concentration, the contribution of instantaneous diffusion to electron spin-echo dephasing would be significant.

In case of a homogeneous distribution in three dimensions, the baseline slope of DEER signal can be used to estimate the local spin concentration using Eqs. (3) and (4) [25–28]:

$$V(t) = \exp(-kt) \quad (3)$$

with

$$k^{-1} = 1.0027 \frac{10^{-3}}{\lambda_{\text{DEER}} C_d}, \quad (4)$$

where $V(t)$ is the time-domain DEER background signal, λ_{DEER} is fraction of spins inverted by the pump pulse in the DEER measurement (usually in the range of 0.2–0.3), and C_d indicates the mean local spin concentration within the effective DEER measurable volume (with a radius of ca. 6 nm, with the instrument setup of the present study). The theoretical curves showing the local concentration change as a function of the slope of DEER background trace are given in the Online Resource (Figure S2). In addition, this study also obtained the interspin distance distributions $P(r)$ by performing the DEER time-domain data analysis using the Tikhonov regularization (TIKR) method based on the L-curve method, followed by a data refinement process using the maximum entropy method [29, 30]. The $P(r)$ results are shown in the Online Resource (Figure S3).

3 Results

Mesoporous silica materials with three different average pore diameters in the range of 7–11 nm (MSU, SBA-15, and SBA-15-p, as detailed in Table 1) were used in the present study. The mesoporous materials exhibit 2D-hexagonal arrangements of pore channels with major differences in particle morphology (Fig. 1). The length of nanochannels in the mesoporous materials was estimated from the SEM images

Fig. 1 Morphologies of mesoporous silica materials by SEM imaging. **a** MSU, rod-shaped with a cross-linked hexagonal pore structure. **b** SBA-15, fiber-like structure with hexagonally ordered pores. **c** SBA-15-p-type materials, platelet morphology with short nanochannels running parallel to the thickness of the hexagonal platelets

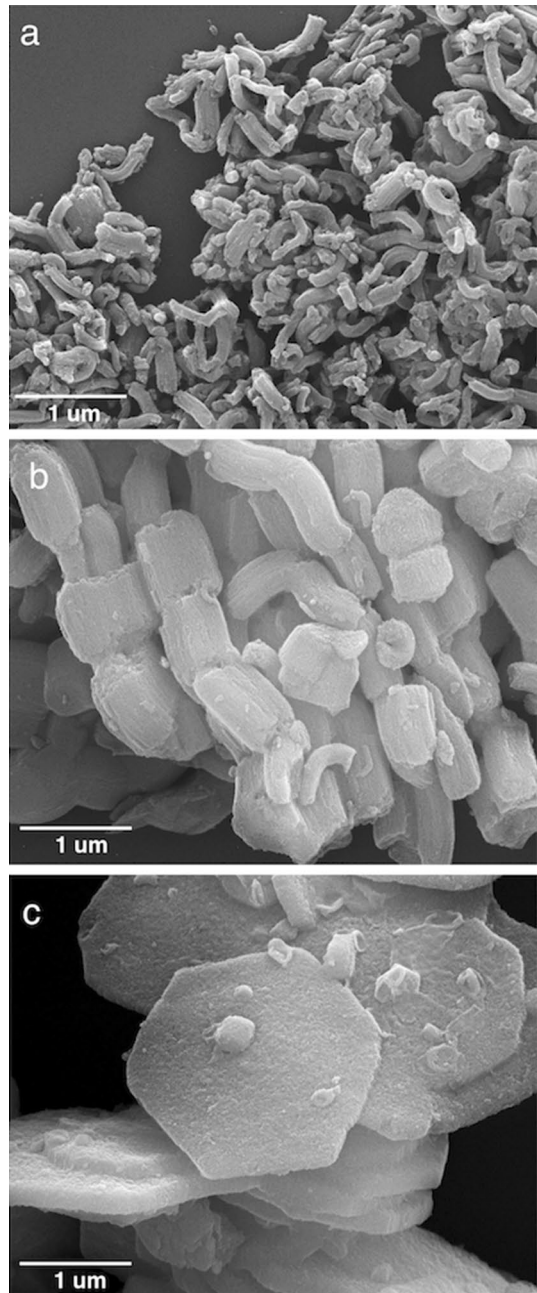


(Fig. 1), displaying the respective lengths in this order: SBA-15 > MSU > SBA-15-p. The channels of SBA-15-p are parallel to the thickness of the hexagonal platelet and are thus the shortest among the three materials studied. As detailed in “[Materials](#)

and Methods”, two spin-labeled polypeptides (i.e., 26-residue-long n3 peptide and 14-mer polyproline) and one spin-labeled protein (i.e., Bid protein) were prepared for the encapsulation in mesoporous materials in the following experiments.

3.1 Study of Double-Labeled n3 Peptides in Mesoporous Materials

To investigate how the DEER background signal of spin-labeled molecules depends on the mesoporous materials, we performed DEER measurements for the double-labeled n3 peptide (n3-d), which exhibits a β -hairpin conformation at pH 6.5 in a

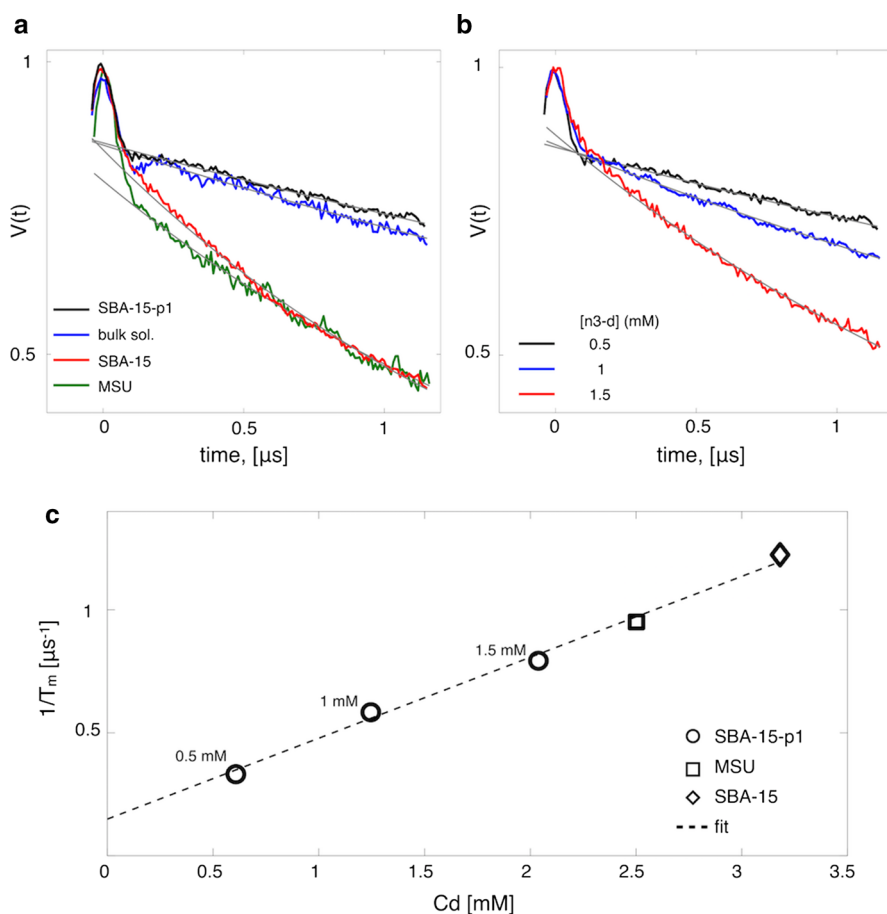


Fig. 2 **a** Time-domain DEER data of spin-labeled n3-d in vitrified bulk solvent versus three different materials, SBA-15-p1, SBA-15, and MSU. Gray lines are the exponentials that best fit the DEER backgrounds. $[\text{n3-d}]$ is fixed at 0.5 mM prior to the encapsulation. **b** Time-domain DEER data of spin-labeled n3-d peptides encapsulated in SBA-15-p1 at varying $[\text{n3-d}]$ from 0.5 to 1.5 mM. **c** Correlation plot of $1/T_m$ versus C_d . C_d is the local spin concentration determined from the DEER background signals. A linear relation (as indicated by dashed line) between $1/T_m$ and C_d is clearly revealed, an important evidence supporting the role of instantaneous diffusion in the measurements

phosphate buffer. It was previously shown by ESR methods that n3 peptide retains most of its hairpin structure when confined in the nanochannels of mesoporous material [15, 17]. The concentration of n3-d peptides ([n3-d]) was fixed at 0.5 mM prior to the encapsulation of the peptide solution into mesoporous materials. Figure 2a shows the DEER time-domain signals of n3-d recorded at 50 K in various conditions, including the vitrified bulk solvent [i.e., the solution containing 30% (v/v) glycerol] and the three mesoporous materials (MSU, SBA-15, and SBA-15-p1). All of the DEER data exhibit a clear modulation depth, which indicates of interspin distances in n3-d, in the early stage of the recorded DEER time evolution, consistent with the expectation that n3-d retains most of its hairpin conformation, whereas the background signals (indicated by gray lines in Fig. 2a) of the DEER measurements are largely different. We found that although the same [n3-d] was prepared prior to the encapsulation, the DEER background signal changes distinctly with the mesoporous materials used. As the DEER background represents the intermolecular dipolar signal, which reflects the spatial distribution of spins in the ESR tube [25, 31], our result indicates that the local spin concentration in the ESR tube depends strongly on the mesoporous materials; the encapsulated peptides are spatially redistributed according to the structure of the host materials. We found that the background trace of SBA-15-p1 is comparable with the result of the bulk solvent and it decays much less rapidly than the results of other materials (SBA-15 and MSU).

The DEER background signals were fitted to the model of homogeneous distribution (Eqs. 3, 4) to estimate the local spin concentrations (i.e., C_d as defined in “Materials and Methods”) after the redistribution of peptides in the materials. C_d values estimated from the analysis of DEER backgrounds are listed in Table 2 together with [spin] (i.e., the given spin concentration calculated from [n3-d] \times 2 \times labeling efficiency), providing a quantitative description of how the local spin concentration C_d is affected by the properties of mesoporous materials. With the same [n3-d] (0.5 mM, approximately equivalent to [spin] \sim 0.75 mM; Table 2), C_d value is estimated to be 3.18, 2.50, and 0.61 mM for SBA-15, MSU, and SBA-15-p1, respectively, in which only the result of SBA-15-p1 is sufficiently close to 0.72 mM, the C_d

Table 2 Experimental conditions and analysis results of n3-d peptides

Mesoporous material	[n3-d] (mM)	[spin] ^a (mM)	C_d (mM)	κ^b	T_m (ns) ^c
SBA-15-p1	0.5	0.75 \pm 0.05	0.61	0.813	3032
SBA-15-p1	1	1.5 \pm 0.1	1.25	0.833	1719
SBA-15-p1	1.5	2.25 \pm 0.15	2.04	0.907	1264
MSU	0.5	0.75 \pm 0.05	2.50	3.333	1052
SBA-15	0.5	0.75 \pm 0.05	3.18	4.240	817
Bulk solution	0.5	0.75 \pm 0.05	0.72	0.960	2838

^aLabeling efficiency of n3-d is in the range of 70–80%

^b κ is calculated from $C_d/[spin]$ to reflect the extent of clustering

^c T_m values are determined from the analysis of pulsed ESE measurements using a stretched exponential function as described in “Materials and Methods”. Estimated errors are about 5–10%

value obtained from the DEER data of bulk solvent. In terms of the extent of spin clustering (i.e., κ , defined by $C_d/[\text{spin}]$), the results indicate that the number of spins within the effective DEER measurable volume in SBA-15 is much greater than in MSU and then SBA-15-p1; the respective κ are 4.24, 3.33, and 0.813. The spatial distribution of n3-d peptides, as reflected by κ or C_d , depends critically on the host materials, suggesting that the shorter is the nanochannel length, the less is κ value.

To verify the above finding concerning SBA-15-p1, we performed DEER measurements for the encapsulation of n3-d into SBA-15-p1 with a fixed volume of n3-d solutions at varying [n3-d] (0.5, 1, and 1.5 mM) (Fig. 2b). We observed that the DEER backgrounds obtained with SBA-15-p1 material change clearly with [n3-d]; the higher the [n3-d], the faster the DEER background decays. It appears that both channel morphology (Fig. 2a) and the concentration of biomolecules (Fig. 2b) affect the DEER background decay.

This study also performed ESE measurements to obtain the phase memory spin–spin relaxation time (T_m ; Table 2) for all of the samples studied. For [n3-d] fixed at 0.5 mM, T_m values (in unit of ns) are 817 (SBA-15), 1052 (MSU), 2838 (bulk solvent), and 3032 (SBA-15-p1). Only in the studies with SBA-15-p1 can we obtain T_m values comparable to the result of bulk solvent. Figure 2c shows a plot of $1/T_m$ versus C_d , revealing clearly a linear correlation between them. The strong dependence of spin–spin relaxation time on local spin concentration (C_d) is considered as an important indication that instantaneous diffusion plays a role in the spin-echo decay, [24, 25] in view of the fact that instantaneous diffusion occurs in cases of high spin concentrations causing dipolar interaction among on-resonant spins (i.e., spins pumped by microwaves) [32, 33]. The linear relationship can be observed for n3-d in the three mesoporous materials studied. It suggests that in the studies with mesoporous materials, the spatial distribution of the encapsulated biomolecules, reflected by C_d or κ , is determined by the textural properties of the materials and that the main spin relaxation mechanism here is instantaneous diffusion.

3.2 Study of Single-Labeled Polyproline Peptides in Mesoporous Materials

To further investigate the spatial distribution of biomolecules in nanochannels, we performed DEER and ESE measurements for single-labeled polyproline peptides (PP-s) in MSU and SBA-15 and compared the results with the bulk solvent study. As PP-s is singly labeled and [PP-s] prior to the encapsulation is fixed (0.5 mM), the only factor that affects the DEER background signal is the spatial distribution of PP-s modulated by the textural properties of mesoporous materials. Figure 3a shows the DEER time-domain signals for [PP-s] 0.5 mM in SBA-15, MSU, and bulk solvent, displaying distinct differences in the DEER background signals. The DEER signals were analyzed to obtain the respective C_d values (Table 3); they are 2.25, 1.23, and 0.39 mM in the following order: SBA-15 > MSU > bulk solution, which coincides with the order of nanochannel lengths for SBA-15 and MSU. The result provides a support for the finding of the n3-d study that the longer the length of nanochannels is used, the greater the C_d value is measured. In other words, we found that spin-labeled molecules in the materials of longer nanochannels tend to become

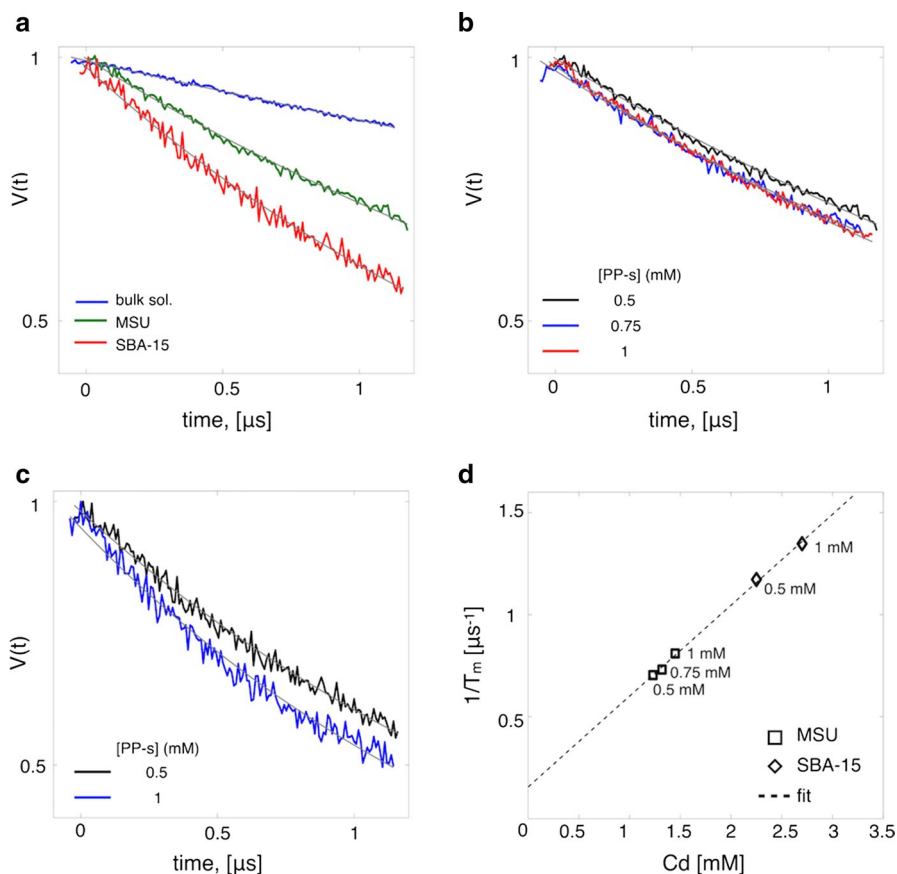


Fig. 3 **a** Time-domain DEER data for single-labeled PP-s peptides in bulk solvent and two different materials, MSU and SBA-15. [PP-s] is fixed at 0.5 mM. The DEER background signals (gray lines) are clearly different between the three conditions. The concentration-dependent DEER results for single-labeled PP-s peptides encapsulated in MSU (**b**) and SBA-15 (**c**). **d** Correlation plot of $1/T_m$ versus C_d . A linear relation between them is clearly revealed

Table 3 Experimental conditions and analysis results of singly labeled PP-s

Mesoporous material	[n3-d] (mM)	[spin] ^a (mM)	C_d (mM)	κ ^b	T_m (ns) ^c
MSU	0.5	0.4 ± 0.025	1.23	3.075	1421
MSU	0.75	0.6 ± 0.375	1.32	2.200	1368
MSU	1	0.8 ± 0.05	1.45	1.825	1235
SBA-15	0.5	0.4 ± 0.025	2.25	5.625	853
SBA-15	1	0.8 ± 0.05	2.7	3.375	742
Bulk solution	0.5	0.4 ± 0.05	0.39	0.975	3543

^aLabeling efficiency of PP-s is in the range of 70–80%

^b κ is calculated from $C_d/[\text{spin}]$ to reflect the extent of clustering

^c T_m values are determined from the analysis of pulsed ESE measurements using a stretched exponential function as described in “Materials and Methods”. Estimated errors are about 5–10%

more clustered, which leads to an increase in the measured local spin concentration C_d . The same observation can be made from κ values as they are 5.625 (SBA-15), 3.075 (MSU), and 0.975 (bulk solvent).

Next, we performed the concentration-dependent DEER measurements ([PP-s] in the range of 0.5–1 mM) with the materials MSU (Fig. 3b) and SBA-15 (Fig. 3c). Interestingly, the DEER background signals were observed to change little with the concentration of spin-labeled molecules, inconsistent with the finding for the SBA-15-p1 study, as shown in Fig. 2b. The observation for the little change in the background decay can be quantitatively described by C_d values as follows. C_d for the MSU study (Fig. 3b) is determined to be 1.23, 1.32, and 1.45 mM when [PP-s] is varied from 0.5 to 0.75 and 1 mM; C_d for the SBA-15 study (Fig. 3c) is determined to be 2.25 and 2.7 mM when [PP-s] is varied from 0.5 to 1 mM. However, C_d obtained for MSU is consistently about half of those obtained for SBA-15. Collectively, the type of the mesoporous materials plays an important role in determining the decay of DEER background signals (reflected by C_d), hence the spatial distribution. In the studies with MSU and SBA-15 materials, PP-s peptides tend to cluster (as reflected by large κ values) and the sensitivity of DEER background signals to local spin concentration is somewhat hampered by the morphologies of the two materials.

T_m of PP-s was measured in the ESE experiment and found to decrease with increasing [spin] of PP-s (Table 3), in good agreement with the result of the n3-d study (Table 2). Likewise, a linear dependence between $1/T_m$ and C_d values (Fig. 3d) is obtained for the PP-s study with MSU and SBA-15 materials. It confirms our earlier finding that instantaneous diffusion is the dominant relaxation mechanism in the studies of mesoporous materials.

3.3 Effects of Pore Size on the Spatial Distribution of Proteins

In the above sections, we report that the decay of DEER background signal reflects [spin] in the study with SBA-15-p1, whereas it becomes insensitive to the change in [spin] when the host material MSU or SBA-15 is used. As the nanochannels of SBA-15-p1 are much shorter in length than those of MSU and SBA-15 materials (Fig. 1), it suggests that the length of nanochannel plays an important role in determining the spatial distribution of spin-labeled molecules in the mesoporous materials and that host materials with shorter nanochannels are more effective in reducing the clustering of spin-labeled molecules (i.e., smaller κ). This study, therefore, prepared more SBA-15-p-type materials with various pore sizes to investigate how the DEER background signal depends on the pore size of mesoporous materials.

A series of SBA-15-p materials with different pore diameters in the range of 6–11 nm (denoted by SBA-15-p2, -p3, -p4, and -p5, as shown in Table 1) were prepared. Bid protein with molecular weight of 22 kDa and geometric dimensions of $3 \times 4 \times 4$ nm (approximately) is used as a model protein (Fig. 4a). As wild-type Bid contains two native cysteine residues, it is directly used to generate double-labeled Bid in the following studies. Figure 4b shows the DEER time-domain signals of double-labeled Bid proteins encapsulated in various mesoporous materials.

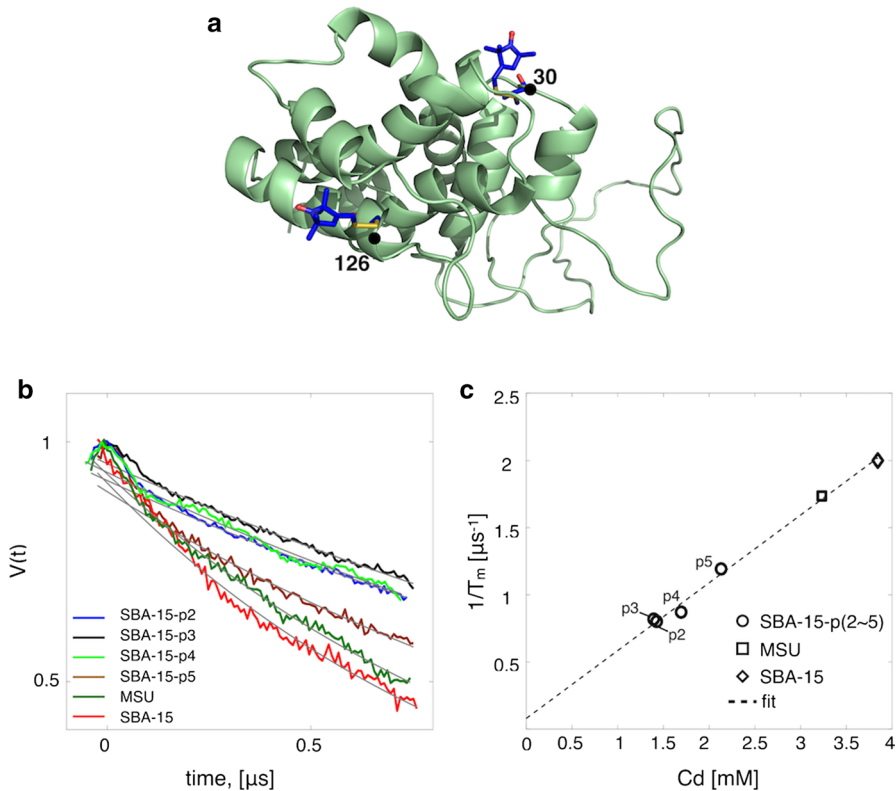


Fig. 4 **a** Structural model of Bid protein (PDB:1DDB) carrying two spin labels at the native cysteine sites (30C and 126C). **b** Time-domain DEER data for spin-labeled Bid protein in six different mesoporous materials, SBA-15-p(2~5), MSU, and SBA-15. [Bid] is fixed at 0.5 mM. **c** Correlation plot of $1/T_m$ versus C_d for the Bid results, exhibiting a clear linear relation

Basically, the DEER data are characterized by a clear modulation depth, verifying the presence of intra-molecular distances in Bid proteins. Importantly, it shows that even though [spin] is fixed (ca. 0.95 mM), the DEER background intermolecular signals exhibit a clear dependence on the pore size of host materials. Specifically, C_d is determined to be 1.43, 1.40, 1.7, and 2.13 mM (Table 4) when average pore diameter of the SBA-15-p-type materials is increased from 6.5, 8.1, 9.1, and 10.4 nm. It suggests that having too large pore diameter (ca. > 10 nm) causes some clustering of Bid proteins, thus leading to the increase in the measured C_d and thus κ . Aside from the result of the largest pore diameter, κ value is sufficiently small in the range of 1.4–1.8. The use of SBA-15-p-type materials is helpful to avoid the molecular clustering upon the encapsulation. The variation in the pore diameter in the range of 6–10 nm seems to affect little to the spatial distribution of the encapsulated proteins. κ values for Bid in MSU or SBA-15 are significantly greater than those obtained from SBA-15-p-type materials. Again, the longer is the length of nanochannels, the greater are the biomolecules clustered.

Table 4 Experimental conditions and analysis results of doubly labeled Bid proteins

Mesoporous material	[Bid] (mM)	[spin] ^a (mM)	C_d (mM)	κ^b	T_m (ns) ^c
SBA-15-p2	0.5	0.95 ± 0.05	1.43	1.682	1251
SBA-15-p3	0.5	0.95 ± 0.05	1.40	1.474	1225
SBA-15-p4	0.5	0.95 ± 0.05	1.7	1.789	1151
SBA-15-p5	0.5	0.95 ± 0.05	2.13	2.242	840
MSU	0.5	0.95 ± 0.05	3.23	3.400	576
SBA-15	0.5	0.95 ± 0.05	3.84	4.042	500

^aLabeling efficiency of Bid proteins is > 95%

^b κ is calculated from $C_d/[\text{spin}]$ to reflect the extent of clustering

^c T_m values are determined from the analysis of pulsed ESE measurements using a stretched exponential function, as described in “Materials and Methods”. Estimated errors are about 5–10%

Figure 4c shows the plot of $1/T_m$ versus C_d values for the study of Bid proteins encapsulated in the mesoporous materials. A linear relation was again found between $1/T_m$ and C_d , providing evidence that instantaneous diffusion is dominant in the study with SBA-15-p-type mesoporous materials.

In summary, the present study has investigated how the spatial distributions of molecules encapsulated in mesoporous materials are affected by the textural properties of host materials using pulsed ESR techniques including DEER and ESE methods. By analyzing the DEER background signals, which reflect intermolecular dipolar interactions within the effective volume of DEER measurement, we are able to quantitatively describe (in terms of C_d) the spatial distribution of spin-labeled biomolecules in the mesoporous materials of interest. Value of C_d corresponds to local spin concentration in the effective volume of DEER measurement. In a regular vitrified solvent, C_d obtained from the DEER background analysis can be shown to be consistent with the given spin concentration [spin]. In the studies with spin-labeled molecules encapsulated in the mesoporous materials such as MSU and SBA-15, we found that the C_d values obtained are approximately 2–6 times greater than the given [spin]. C_d being too much greater than [spin] indicates that the spin-labeled biomolecules are not only redistributed according to the mesoporous structures, but also clustered in the local environment of the host materials. The results of the present study show that preparing host materials with shorter channel length is an effective way to reduce the clustering of molecules, which consequently makes κ close to unity. As biomolecules, once encapsulated in the mesoporous materials, were previously shown to diffuse extremely slowly [12, 13], it is reasonable to find that preparing host materials with long channel length does little help to increase the capacity. Besides, this study found that increasing pore diameter of the host material causes little change to the clustering of spin-labeled proteins, provided that the pore size is sufficient to accommodate the guest biomolecules.

SBA-15-p-type materials have unique hexagonal platelet morphologies with short channels (ca. 200 nm) running parallel to the thickness of the hexagonal platelet. Previously, the textural properties of SBA-15-p-type materials have been demonstrated effective in increasing the uptake rate of organic molecules and proteins as

compared to other conventional fiber-like SBA-15 materials [34–36]. In the present study, we show that the use of SBA-15-p-type materials could be a potentially useful approach to improve the measurement of pulsed dipolar spectroscopy. In the n3-d studies with SBA-15-p1 (Table 2), κ values are consistently less than unity when [spin] is increased from 0.75 to 1.5, and 2.25 mM; the corresponding T_m values are 3032, 1719, and 1264 ns, whereas T_m of the bulk solvent measurement (0.5 mM) is ca. 2838 ns. In the studies of Bid proteins, the T_m values (> 1200 ns) for SBA-15-p2 and -p3 are comparable to that (ca. 1200 ns) obtained in bulk solvent. The results indicate that it is possible to modulate the spatial distribution of spin-labeled biomolecules and reduce local molecular clustering (which, consequently, leads to suppression of instantaneous diffusion and thus an increase in T_m) by changing the textural properties (e.g., channel length) of mesoporous materials. The reduction in C_d , which leads to an increase in T_m , can be achieved by shortening the length of nanochannels and, as a result, enables a longer evolution time in the DEER signals. This study has opened a possibility of improving the measurements of pulsed dipolar spectroscopy by modulating textural properties of mesoporous materials.

Finally, we note that this methodology is good for small peptides or proteins that their secondary structure is not altered by the encapsulation into mesopores. The assessment presented here has provided valuable information for future experimental studies on biomolecules under nanoconfinement.

4 Conclusions

This study has assessed the use of mesoporous silica materials to improve pulsed dipolar spectroscopy. First, this study investigated how the spatial distribution of spin-labeled biomolecules is affected by the textural properties (e.g., nanochannel length, pore diameter, and nanoparticle morphology) of mesoporous materials. Our results suggest that the spatial distribution of the encapsulated biomolecules depends critically on the length of nanochannels. Basically, the shorter the nanochannel length, the less the extent of the biomolecular clustering in the materials, likely because that with the same amount of the nanoparticles, the smaller the size of the individual host nanoparticles, the greater number of the available pores to accommodate the guest molecules and thus avoid the clustering of biomolecules in the materials. This study demonstrates that instantaneous diffusion is the major contributor to the spin–spin relaxation mechanism in mesoporous materials. To suppress the unwanted instantaneous diffusion in the measurements with mesoporous materials, one should focus on reducing the biomolecular clustering through the modulation of the textural properties (e.g., channel length and nanoparticle size) of materials. Although the spatial distribution is also affected by the size of the encapsulated biomolecules, it is possible that with an appropriate combination of the mesoporous materials and biomolecules, the spatial distribution of the guest molecules could be homogeneous and well separated such that the phase memory spin–spin relaxation time is longer than that obtained in the conventional bulk solvent. With a longer T_m , the sensitivity of pulsed dipolar spectroscopy can be improved.

Acknowledgements This work was supported by Grants from the Ministry of Science and Technology of Taiwan (105-2628-M-007-005 and 106-2627-M-007-009) and the Frontier Research Center on Fundamental and Applied Sciences of Matters at NTHU. All of the CW/pulse ESR measurements were conducted in the Research Instrument Center of Taiwan located at NTHU.

References

1. J. Liu, Q.H. Yang, C. Li, *Chem. Commun.* **51**, 13731–13739 (2015)
2. S. Mitragotri, P.A. Burke, R. Langer, *Nat. Rev. Drug Discov.* **13**, 655–672 (2014)
3. S. Isaksson, E.B. Watkins, K.L. Browning, T.K. Lind, M. Cardenas, K. Hedfalk, F. Hook, M. Andersson, *Nano Lett.* **17**, 476–485 (2017)
4. S. Matsuura, M. Chiba, T. Tsunoda, A. Yamaguchi, *J. Nanosci. Nanotechnol.* **18**, 104–109 (2018)
5. B.W. Chen, W. Qi, X.L. Li, C.H. Lei, J. Liu, *Small* **9**, 2228–2232 (2013)
6. C.H. Lee, T.S. Lin, C.Y. Mou, *Nano Today* **4**, 165–179 (2009)
7. S. Hudson, J. Cooney, E. Magner, *Angew. Chem. Int. Ed.* **47**, 8582–8594 (2008)
8. N. Carlsson, H. Gustafsson, C. Thorn, L. Olsson, K. Holmberg, B. Akerman, *Adv. Colloid Interface Sci.* **205**, 339–360 (2014)
9. M.R. Fleissner, M.D. Bridges, E.K. Brooks, D. Cascio, T. Kalai, K. Hideg, W.L. Hubbell, *Proc. Natl. Acad. Sci. USA* **108**, 16241–16246 (2011)
10. J.S. Tong, P.P. Borbat, J.H. Freed, Y.K. Shin, *Proc. Natl. Acad. Sci. USA* **106**, 5141–5146 (2009)
11. S.Y. Park, P.P. Borbat, G. Gonzalez-Bonet, J. Bhatnagar, A.M. Pollard, J.H. Freed, A.M. Bilwes, B.R. Crane, *Nat. Struct. Mol. Biol.* **13**, 400–407 (2006)
12. C.J. Tsai, Y.W. Chiang, *J. Phys. Chem. C* **116**, 19798–19806 (2012)
13. Y.C. Lai, Y.F. Chen, Y.W. Chiang, *PLoS ONE* **8**, e68264 (2013)
14. K.J. Chang, Y.H. Kuo, Y.W. Chiang, *J. Phys. Chem. B* **121**, 4355–4363 (2017)
15. Y.W. Huang, Y.C. Lai, C.J. Tsai, Y.W. Chiang, *Proc. Natl. Acad. Sci. USA* **108**, 14145–14150 (2011)
16. S.A. Kozin, G. Bertho, A.K. Mazur, H. Rabesona, J.P. Girault, T. Haertle, M. Takahashi, P. Debey, G.H.B. Hoa, *J. Biol. Chem.* **276**, 46364–46370 (2001)
17. Y.W. Huang, Y.W. Chiang, *Phys. Chem. Chem. Phys.* **13**, 17521–17531 (2011)
18. K.J. Oh, S. Barbutto, N. Meyer, R.S. Kim, R.J. Collier, S.J. Korsmeyer, *J. Biol. Chem.* **280**, 753–767 (2005)
19. Y.H. Kuo, Y.R. Tseng, Y.W. Chiang, *Langmuir* **29**, 13865–13872 (2013)
20. C.H. Liu, C.Y. Lin, J.L. Chen, N.C. Lai, C.M. Yang, J.M. Chen, K.T. Lu, *J. Catal.* **336**, 49–57 (2016)
21. P.H. Ku, C.Y. Hsiao, M.J. Chen, T.H. Lin, Y.T. Li, S.C. Liu, K.T. Tang, D.J. Yao, C.M. Yang, *Langmuir* **28**, 11639–11645 (2012)
22. M. Pannier, S. Veit, A. Godt, G. Jeschke, H.W. Spiess, *J. Magn. Reson.* **142**, 331–340 (2000)
23. A. Zecevic, G.R. Eaton, S.S. Eaton, M. Lindgren, *Mol. Phys.* **95**, 1255–1263 (1998)
24. R. Dastvan, B.E. Bode, M.P. Karupiah, A. Marko, S. Lyubanova, H. Schwalbe, T.F. Prisner, *J. Phys. Chem. B* **114**, 13507–13516 (2010)
25. P.P. Borbat, J.H. Freed, *Methods Enzymol.* **423**, 52–116 (2007)
26. G. Jeschke, S. Schlick, *Phys. Chem. Chem. Phys.* **8**, 4095–4103 (2006)
27. S. Ruthstein, A.M. Raitsimring, R. Bitton, V. Frydman, A. Godt, D. Goldfarb, *Phys. Chem. Chem. Phys.* **11**, 148–160 (2009)
28. S. Ruthstein, A. Potapov, A.M. Raitsimring, D. Goldfarb, *J. Phys. Chem. B* **109**, 22843–22851 (2005)
29. Y.W. Chiang, P.P. Borbat, J.H. Freed, *J. Magn. Reson.* **177**, 184–196 (2005)
30. Y.W. Chiang, P.P. Borbat, J.H. Freed, *J. Magn. Reson.* **172**, 279–295 (2005)
31. E.R. Georgieva, A.S. Roy, V.M. Grigoryants, P.P. Borbat, K.A. Earle, C.P. Scholes, J.H. Freed, *J. Magn. Reson.* **216**, 69–77 (2012)
32. A.A. Nevzorov, J.H. Freed, *J. Chem. Phys.* **115**, 2401–2415 (2001)
33. K.M. Salikhov, S.A. Dzuba, A.M. Raitsimring, *J. Magn. Reson.* **42**, 255–276 (1981)
34. S.Y. Chen, C.Y. Tang, W.T. Chuang, J.J. Lee, Y.L. Tsai, J.C.C. Chan, C.Y. Lin, Y.C. Liu, S.F. Cheng, *Chem. Mater.* **20**, 3906–3916 (2008)
35. M. Ferdousi, M. Pazouki, F.A. Hessari, M. Kazemzad, *J. Porous Mater.* **23**, 453–463 (2016)
36. S.Y. Chen, Y.T. Chen, J.J. Lee, S. Cheng, *J. Mater. Chem.* **21**, 5693–5703 (2011)